Chirp Parameter Selected Mapping for Low PAPR AFDM Transmission

Zunqi Li, Graduate Student Member, IEEE, Xiaojie Fang, Member, IEEE, Xuejun Sha, Member, IEEE, and Dirk T. M. Slock, Life Fellow, IEEE

Abstract—Affine frequency division multiplexing (AFDM) has recently emerged as a promising multicarrier waveform for high-mobility and doubly selective channels. However, similar to orthogonal frequency division multiplexing (OFDM), AFDM signals suffer from a high peak-to-average power ratio (PAPR), which limits the efficiency of radio frequency (RF) power amplifiers. To address this issue, we propose a chirp parameter selected mapping (CSM) scheme that exploits the tunable chirp parameter of AFDM to generate multiple candidate signals and selects the one with the lowest PAPR for transmission, thereby achieving low-PAPR signal generation without introducing waveform extensions. A theoretical lower bound on the complementary cumulative distribution function (CCDF) of CSM is established under the independence assumption, which exhibits an exponential tail decay with the selection order. Accordingly, both a candidate design criterion and a practical guideline are developed to minimize the cross-correlation between signals. Simulation results show that the proposed CSM scheme approaches the theoretical bound and achieves significant PAPR reduction over existing baselines, while maintaining error-rate performance in doubly selective channels.

Index Terms—Affine frequency division multiplexing, peak-to-average power ratio, selected mapping, low-correlation candidate design.

I. Introduction

S the world moves toward the vision of sixth-generation (6G) networks, the ultimate goal is to achieve seamless communication across land, sea, air, and space, thereby enabling a truly interconnected Internet of Everything. High-mobility scenarios such as vehicle-to-everything (V2X), unmanned aerial vehicles (UAVs), autonomous ships, high-speed rail, and low Earth orbit (LEO) satellites are expected to play a central role in this vision [1]. Unlike static environments, these scenarios involve rapid channel variations and complex propagation, where conventional transceiver designs often struggle to maintain reliable and efficient links. In particular, severe multipath propagation combined with pronounced Doppler shifts gives rise to doubly selective channels, which pose a fundamental challenge to system performance.

This work was supported in part by the National Natural Science Foundation of China (Grant U23A20278), in part by the National Key Research and Development Program of China (Grant 2022YFB2902404) and in part by the China Scholarship Council. The corresponding author is Xiaojie Fang.

Zunqi Li and Xiaojie Fang are with the School of Electronics and Information Engineering, Harbin Institute of Technology, Harbin, China, and the National Key Laboratory of Advanced Communication Networks, Shijiazhuang, China. Xuejun Sha is with the School of Electronics and Information Engineering, Harbin Institute of Technology, Harbin, China (e-mail: {lizunqi@stu., fangxiaojie@, shaxuejun@}hit.edu.cn).

Dirk Slock is with the Department of Communication Systems, EURE-COM, 06410 Biot, France (e-mail: Dirk.Slock@eurecom.fr).

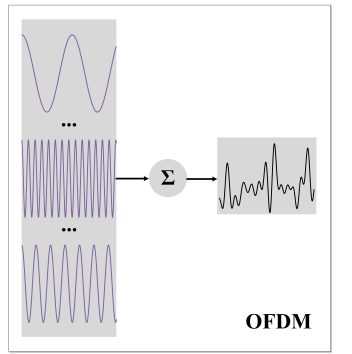
A. Related work

As a promising multicarrier waveform candidate, Affine Frequency Division Multiplexing (AFDM) has demonstrated strong robustness in high-mobility and doubly dispersive environments. By constructing its signals from orthogonal chirp basis functions, AFDM inherits a distinctive capability of chirp parameter tunability. This flexibility enables flexible spreading of the signal energy across the time–frequency plane, thereby enhancing resilience to fading and interference. The theoretical foundations of AFDM are now well established. In [2], an equivalent affine frequency-domain channel model was derived, showing that AFDM can achieve full path diversity under maximum-likelihood detection. Later, [3] extended the analysis to linear equalization and demonstrated that AFDM can approach equal-SINR transmission across subcarriers, indicating its potential for low-complexity iterative receiver design.

Apart from these error-rate advantages, AFDM also offers improved spectral efficiency. As shown in [2], [4], AFDM requires fewer guard intervals than Orthogonal Time Frequency Space modulation (OTFS), thereby mitigating pilot-data interference and allowing more data to be accommodated within each block. AFDM has also been combined with advanced transmission schemes, such as generalized spatial modulation and sparse code multiple access [6], [7], where it consistently achieves better bit-error-rate (BER) performance than OTFS in high-mobility scenarios. Moreover, AFDM is also well aligned with the key visions of 6G. In integrated sensing and communications, it offers fine delay-Doppler resolution, which enables accurate joint sensing and communication [8]-[10]. Its robustness has also been demonstrated in non-terrestrial networks [11], further underscoring AFDM's versatility for next-generation wireless systems.

Nevertheless, in the diverse Internet of Everything ecosystem, many devices operate with nonlinear and low-efficiency radio frequency (RF) chains, unlike the highly linear and efficient ones used at base stations. This limitation is particularly problematic for multicarrier transmission such as OFDM and AFDM, which are intrinsically prone to high peak-to-average power ratio (PAPR), as illustrated in Fig.1. Consequently, PAPR becomes a critical bottleneck for reliable and energy-efficient transmission in such devices. In multicarrier systems, high PAPR typically leads to several detrimental effects. First, it forces the power amplifier (PA) to operate with a large input back-off, which drastically reduces power efficiency and degrades overall spectral efficiency [12]–[14]. Second,

1



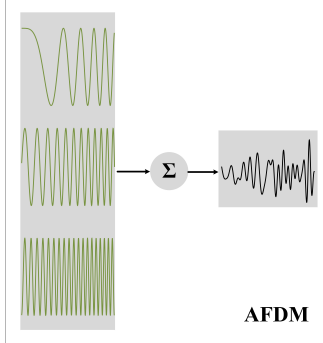


Fig. 1: Superposition of multiple subcarriers leading to high PAPR

when the back-off is insufficient, the PA enters its nonlinear region, causing in-band distortion that increases error vector magnitude (EVM) and degrades link reliability [15]–[17]. Third, nonlinear distortion produces out-of-band spectral regrowth, which elevates the adjacent channel leakage ratio and may cause harmful interference to coexisting systems [16], [18], [19]. Finally, high PAPR enlarges the dynamic-range requirements of analog front-end components such as DACs, ADCs, and linearization units, thereby raising hardware cost and design complexity, and scaling unfavorably in multiantenna or massive-access deployments [12], [13], [20].

In multicarrier systems, extensive research has been devoted to PAPR reduction schemes for OFDM over the past two decades. Representative approaches include clipping/companding, partial transmit sequence (PTS), precoding, and selective mapping (SLM). Clipping and companding are attractive for their simplicity, but they are distortion-based and inevitably cause in-band EVM degradation and out-ofband spectral regrowth [21], [22]. PTS achieves stronger PAPR reduction by optimizing the phases of multiple subblocks, but its combinatorial search complexity and large side-information (SI) overhead limit practical feasibility [23]–[25]. Precodingbased schemes can suppress envelope fluctuations without requiring SI, yet they alter the inherent time-frequency resource mapping of OFDM, and such waveform extensions inevitably introduce new trade-offs between complexity, flexibility, and performance [26]-[28]. In contrast, SLM has emerged as a widely adopted distortion-free baseline: it preserves the receiver structure but requires the transmission of additional SI to indicate the selected candidate. With properly protected SI, SLM achieves progressively better PAPR reduction as the number of candidates increases [29], [30].

The candidate-selection principle from SLM has also inspired investigations in chirp-based multicarrier systems. For Orthogonal Chirp Division Multiplexing (OCDM), a straightforward dual-candidate scheme can be obtained by switching between positive and negative chirp slopes [31]. While this design provides a certain degree of PAPR reduction, its effectiveness is fundamentally constrained by the extremely limited candidate set. Beyond OCDM, researchers have recently proposed PAPR-reduction strategies tailored to AFDM. One representative approach is grouped pre-chirp selection

(GPS) [32], where the pre-chirp parameter is varied in a group-wise manner across subcarriers to form multiple candidates, and the candidate with the lowest PAPR is selected for transmission. However, GPS does not sufficiently exploit the correlation among candidates, so under limited side information the achievable PAPR reduction is restricted. In addition, weighted affine Fourier transform based hybrid-carrier (HC-WAFT) [33] has been proposed, which superimposes single-carrier components onto AFDM blocks within a WAFT framework. While effective in lowering PAPR, HC-WAFT introduces noticeable error-rate degradation in doubly selective channels.

B. Motivation and Contributions

As discussed in the preceding section, prior works focus on extending AFDM through grouped designs or weighted multi-component extensions, but they have not fully explored the potential of AFDM's inherent chirp parameters for candidate selection. This built-in flexibility makes selective mapping straightforward, without the burden of generating or storing large sets of phase sequences. Building on this insight, we design a low-PAPR transmission scheme tailored for AFDM. The main contributions are summarized as follows:

- We propose a chirp parameter selected mapping (CSM) scheme for AFDM, which exploits multiple chirp parameter candidates to achieve effective PAPR reduction while fully preserving the original AFDM signal structure.
- We derive the complementary cumulative distribution function (CCDF) of AFDM using an asymptotic Gaussian approximation, and further establish a lower bound for AFDM-CSM under the independence assumption.
- We prove that the ideal lower bound cannot be achieved in practice, and, based on the properties of generalized quadratic Gauss sums (GQGS), we develop a more practical design principle together with an illustrative example.
- We validate the proposed AFDM-CSM scheme through extensive simulations. Results show that AFDM-CSM can closely approach the theoretical CCDF lower bound without requiring any waveform extensions, thereby confirming its effectiveness and efficiency.

C. Organization and Notation

The rest of this paper is organized as follows. Section III provides preliminaries on AFDM and the PAPR metric. Section III introduces the proposed CSM scheme and its lower bound analysis. Section IV discusses candidate design criteria and practical guidelines. Simulation results are presented in Section V, followed by conclusions in Section VI.

We use b to denote a scalar, \mathbf{b} a vector, and \mathbf{B} a matrix. \mathbf{I}_N and $\mathbf{0}_N$ represent the $N \times N$ identity and zero matrices, respectively, while \mathbf{F}_N denotes the N-point discrete Fourier transform (DFT) matrix. The notation $(\cdot)^{\mathrm{H}}$ indicates the conjugate transpose, and $(\cdot)^n$ the n-th power. The operators $\lfloor b \rfloor$ and $\lceil b \rceil$ denote the floor and ceiling of b, respectively. For a matrix \mathbf{B} , $\mathbf{B}_{(i,j)}$ denotes its (i,j)-th entry, and for a vector \mathbf{b} , $\mathbf{b}_{(i)}$ denotes its i-th element. We use $\mathbb{E}[\cdot]$ for expectation, $\gcd(\cdot,\cdot)$ for the greatest common divisor, $a \mid b$ and $a \nmid b$ to indicate that a divides and does not divide b, respectively, and $a \equiv b$

(mod n) to denote congruence modulo n. The symbols $\Re\{\cdot\}$ and $\Im\{\cdot\}$ denote the real and imaginary parts, respectively, and $\delta_{i,j}$ denotes the Kronecker delta. Finally, $\mathcal{CN}(\mu, \sigma^2)$ stands for a circularly symmetric complex Gaussian random variable with mean μ and variance σ^2 .

II. PRELIMINARIES

In this section, the fundamental concepts of AFDM and the definition of PAPR are reviewed, forming the basis for the subsequent analysis.

A. AFDM

AFDM is a novel multicarrier system that maps information onto multiple orthogonal chirp subcarriers. Compared with conventional OFDM, which performs modulation in the frequency domain, AFDM achieves superior time–frequency spreading, thereby providing enhanced resilience against interference and fading.

At the transmitter, the digital implementation relies on the inverse discrete affine Fourier transform (IDAFT). The IDAFT generalizes the conventional IFFT by introducing two chirp parameters, c_1 and c_2 , which introduce additional quadratic phase modulation. Specifically, c_1 serves as the channel-side parameter, influencing how the signal interacts with time–frequency dispersion, while acts as the signal-side parameter. The resulting time-domain signal $s \in \mathbb{C}^{N \times 1}$ can be represented as a weighted sum of chirp subcarriers. Specifically, the m-th time-domain sample is given by

$$\mathbf{s}_{(m)} = \frac{1}{\sqrt{N}} \sum_{n=0}^{N-1} \mathbf{x}_{(n)} e^{j2\pi(c_1 n^2 + \frac{1}{N}mn + c_2 m^2)}, \qquad (1)$$

where $\mathbf{x} \in \mathbb{C}^{N \times 1}$ denotes an N-length PSK/QAM symbol vector. The entries of \mathbf{x} are modeled as independent and identically distributed (i.i.d.) random variables with zero mean and variance σ_x^2 .

The expression in (1) can be further expressed in the following matrix form:

$$\mathbf{s} = \mathbf{A}^{\mathrm{H}} \mathbf{x} = \mathbf{\Lambda}_{c_1}^{\mathrm{H}} \mathbf{F}_N^{\mathrm{H}} \mathbf{\Lambda}_{c_2}^{\mathrm{H}} \mathbf{x}. \tag{2}$$

where $\Lambda_c = \mathrm{diag}(e^{-j2\pi cn^2}, n=0,1,\ldots,N-1) \in \mathbb{C}^{N\times N}$. At the receiver, the discrete affine Fourier transform (DAFT) is applied for demodulation. Since this paper's primary focus is on the PAPR of the transmitted signal, receiver-side processing is not discussed in detail.

Moreover, the AFDM system usually introduces a chirp-periodic cyclic prefix (CCP) to mitigate multipath effects and inter-block interference. For analytical simplicity, it is typically assumed that N is even and $2Nc_1 \in \mathbb{Z}$, so that the CCP becomes equivalent to the conventional cyclic prefix. Hence, the introduction of CCP can be regarded as a structural extension of the signal, without affecting the subsequent PAPR analysis [34]. According to the chirp periodicity [35], the CCP of length N_{CP} is defined as

$$\mathbf{s}_{(n_{\text{cp}})} = \mathbf{s}_{(N+n_{\text{cp}})} e^{-j2\pi c_1(N^2+2Nn_{\text{cp}})}, n_{\text{cp}} = -N_{\text{CP}}, \cdots, -1.$$

B. PAPR

PAPR is an important metric that quantifies the envelope fluctuations of the transmitted signal, and it is defined as the ratio between the maximum instantaneous power and the average power.

For the discrete-time baseband signal s, sampled at the Nyquist rate, the PAPR is defined as

$$\mathcal{P}(\mathbf{s}) \triangleq \frac{\max_{0 \le n \le N-1} |\mathbf{s}_{(n)}|^2}{\mathbb{E}\{|\mathbf{s}_{(n)}|^2\}}.$$
 (4)

With the unitarity of the DAFT, i.e., $A^HA = I$, we have

$$\mathbb{E}\{\mathbf{s}\mathbf{s}^{H}\} = \mathbf{A}\,\mathbb{E}\{\mathbf{x}\mathbf{x}^{H}\}\,\mathbf{A}^{H} = \sigma_{x}^{2}\mathbf{A}\,\mathbf{I}_{N}\,\mathbf{A}^{H} = \sigma_{x}^{2}\mathbf{I}_{N}.$$
 (5)

Hence, the average AFDM symbol power is

$$\mathbb{E}\{|\mathbf{s}_{(n)}|^2\} = \left[\mathbb{E}\{\mathbf{s}\mathbf{s}^H\}\right]_{(n,n)} = \sigma_x^2.$$
 (6)

Assuming normalized average symbol power for simplicity, the PAPR expression reduces to

$$\mathcal{P}(\mathbf{s}) = \max_{0 \le n \le N-1} |\mathbf{s}_{(n)}|^2. \tag{7}$$

The performance of a PAPR reduction scheme is typically characterized in terms of the CCDF of the PAPR. For a threshold γ , the CCDF is defined as

$$\bar{F}_{\mathcal{P}}(\gamma) \triangleq \Pr \left\{ \mathcal{P}(\mathbf{s}) > \gamma \right\},$$
 (8)

which quantifies the probability that the PAPR of the transmitted signal exceeds γ .

Since both the DFT matrix \mathbf{F}_N and the DAFT matrix \mathbf{A} have entries with unit magnitude scaling (i.e., $1/\sqrt{N}$), the contribution of each data symbol is uniformly distributed in magnitude. This observation allows the well-known PAPR results derived for OFDM to be naturally extended to AFDM systems.

By the central limit theorem (CLT), when N is large, $\Re\{\mathbf{s}_{(n)}\}$ and $\Im\{\mathbf{s}_{(n)}\}$ can be approximated as mutually uncorrelated Gaussian random variables with zero mean and variance 1/2. Consequently, the instantaneous power

$$|\mathbf{s}_{(n)}|^2 = \Re{\{\mathbf{s}_{(n)}\}}^2 + \Im{\{\mathbf{s}_{(n)}\}}^2$$
 (9)

follows an asymptotic chi-square distribution with 2 degrees of freedom. Equivalently, the amplitude $|\mathbf{s}_{(n)}|$ follows a asymptotic Rayleigh distribution, whose probability density function (PDF) is

$$f_r(r) = 2re^{-r^2}, \qquad r \ge 0.$$
 (10)

Assuming that the time-domain samples are approximately independent for large N, i.e., asymptotically independent, the CCDF of PAPR exceeding a threshold γ for AFDM can be approximated as

$$\bar{F}_{\mathcal{P}}(\gamma) = 1 - \prod_{n=0}^{N-1} \Pr\{|\mathbf{s}_{(n)}|^2 \le \gamma\}$$

$$= 1 - (1 - e^{-\gamma})^N, \qquad (11)$$

where the exponential term arises from the Rayleigh distribution of the amplitude.

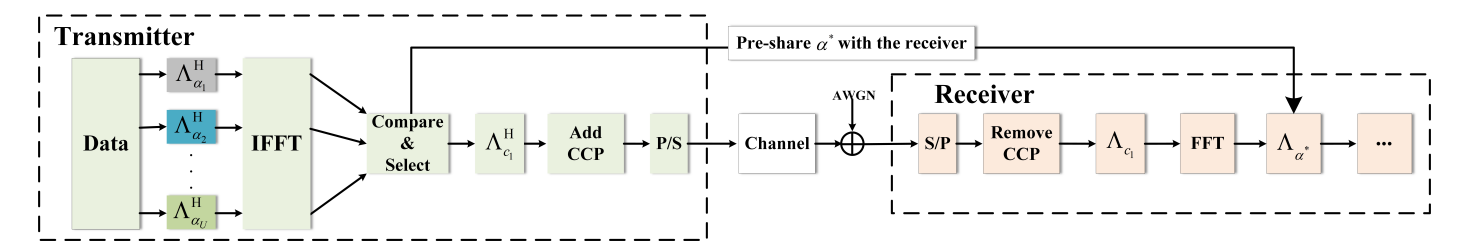


Fig. 2: Block diagram of the AFDM-CSM transceiver.

Throughout the following analysis, we assume N is sufficiently large such that the asymptotic Gaussianity and independence approximations hold, and this assumption will not be repeated henceforth.

III. CHIRP PARAMETER SELECTED MAPPING

A. Chirp Parameter Selected Mapping

As shown in (2), for a given deterministic data sequence \mathbf{x} , the parameters c_1 and c_2 jointly define the transmitted time-domain signal. The phase rotation induced by c_1 occurs after the IDFT operation, affecting only the signal phase and therefore cannot be exploited to reduce the PAPR. In contrast, the phase rotation introduced by c_2 alters the superposition of the complex exponentials in the IDFT, which can potentially change the peak amplitudes and hence the PAPR.

This observation naturally motivates a PAPR reduction scheme based on the selection of c_2 , hereafter referred to as CSM, analogous to the SLM scheme widely used in OFDM systems. In contrast to [32], [33], our scheme avoids waveform extensions and instead achieves PAPR gain while preserving the original AFDM signal structure through the selection of c_2 . Specifically, let $\mathcal{A} = \{\alpha_1, \alpha_2, \dots, \alpha_U\} \subset \mathbb{R}$ denote a set of candidate c_2 parameters. For a given deterministic data sequence \mathbf{x} , each candidate $\alpha_u \in \mathcal{A}$ generates a corresponding time-domain signal

$$\mathbf{s}_{u} = \mathbf{\Lambda}_{c_{1}}^{\mathrm{H}} \mathbf{F}_{N}^{\mathrm{H}} \mathbf{\Lambda}_{\alpha_{u}}^{\mathrm{H}} \mathbf{x}, \quad u = 1, 2, \dots, U,$$
 (12)

all of which share the same amplitude-invariant relation with c_1 , i.e., the final transmitted signals for any c_1 candidate will have the same PAPR as \mathbf{s}_u . Therefore, c_1 can be freely selected based on channel conditions to optimize equalization performance without affecting the PAPR reduction.

By computing the PAPR of each candidate s_u , the transmitter selects the c_2 value that minimizes the PAPR:

$$\alpha^* = \arg\min_{\alpha_u \in \mathcal{A}} \mathcal{P}(\mathbf{s}_u). \tag{13}$$

The signal corresponding to α^* is then transmitted, achieving reduced PAPR.

The overall process is illustrated in Fig. 2. As c_1 has no effect on PAPR (as discussed earlier), the minimum-PAPR decision can be performed prior to the c_1 phase-rotation module. Thus, the c_1 rotation needs to be applied only once to the finally selected candidate, resulting in a saving of (U-1)N complex multiplications per AFDM symbol.

Note that the transmitter needs to transmit the selected c_2 value to the receiver, similar to the SI required in conventional

OFDM SLM scheme. In practice, this can be implemented by sending a small number of bits indicating the index of the chosen candidate in A, ensuring correct demodulation without affecting the PAPR reduction performance.

B. Lower Bound Analysis of CSM

We first reformulate the exceedance event of CSM in a general set-theoretic form. For a threshold γ , define the event

$$B_{u}(\gamma) \triangleq \{ \mathcal{P}(\mathbf{s}_{u}) \leq \gamma \} = \bigcap_{n=0}^{N-1} \{ |\mathbf{s}_{u(n)}|^{2} \leq \gamma \}, \quad (14)$$

which corresponds to the event where the PAPR of the u-th candidate does not exceed γ .

Accordingly, the CCDF of CSM can be written as

$$\bar{F}_{\mathcal{P}}^{\text{CSM}}(\gamma) = \Pr\left\{ \min_{u=1,\dots,U} \mathcal{P}(\mathbf{s}_u) > \gamma \right\}$$

$$= 1 - \Pr\left(\bigcup_{u=1}^{U} B_u(\gamma) \right), \tag{15}$$

where the second equality follows from De Morgan's law and the complement rule of probability.

The union probability in (15) can be evaluated using the inclusion–exclusion principle:

$$\Pr\left(\bigcup_{u=1}^{U} B_u(\gamma)\right) = \sum_{w=1}^{U} c_w \sum_{\substack{\mathcal{I} \subseteq \mathcal{U} \\ |\mathcal{I}| = w}} \Pr\left(\bigcap_{u \in \mathcal{I}} B_u(\gamma)\right), \quad (16)$$

where $U = \{1, 2, ..., U\}$ and $c_w = (-1)^{w+1}$. As an illustrative example, for U = 3 and w = 2, the expansion contains 3 pairwise terms:

$$\sum_{\mathcal{I} \subseteq \mathcal{U} |\mathcal{I}|=2} \Pr \left(\bigcap_{u \in \mathcal{I}} B_u(\gamma) \right) = \Pr \left(B_1(\gamma) \cap B_2(\gamma) \right) + \Pr \left(B_1(\gamma) \cap B_3(\gamma) \right) + \Pr \left(B_2(\gamma) \cap B_3(\gamma) \right).$$

For any $\mathcal{I} \subseteq \mathcal{U}$ with $|\mathcal{I}| = w$,

$$\Pr\left(\bigcap_{u\in\mathcal{I}} B_u(\gamma)\right) = \Pr\left(\bigcap_{u\in\mathcal{I}} \bigcap_{n=0}^{N-1} \{ |\mathbf{s}_{u(n)}|^2 \le \gamma \} \right), \quad (17)$$

namely, the probability that all wN time-domain samples (from w candidates, each with N samples) satisfy the threshold simultaneously.

To analyze (17), we now stack the wN instantaneous samples under consideration into a single vector

$$\mathbf{s}_{\mathcal{I}} \triangleq \left[\left\{ \mathbf{s}_{u(n)} \right\}_{n=0,\dots,N-1} \right]^{\mathrm{T}} \in \mathbb{C}^{wN \times 1}. \tag{18}$$

The correlation matrix of $s_{\mathcal{I}}$ is defined as

$$\mathbf{R}_{\mathcal{I}} \triangleq \mathbb{E}\{\mathbf{s}_{\mathcal{I}}\mathbf{s}_{\mathcal{I}}^{\mathrm{H}}\} \in \mathbb{C}^{wN \times wN},$$

which admits a natural $w \times w$ block structure with $N \times N$ submatrices:

$$\mathbf{R}_{\mathcal{I}} = \begin{bmatrix} \mathbf{R}_{11} & \mathbf{R}_{12} & \cdots & \mathbf{R}_{1w} \\ \mathbf{R}_{21} & \mathbf{R}_{22} & \cdots & \mathbf{R}_{2w} \\ \vdots & \vdots & \ddots & \vdots \\ \mathbf{R}_{w1} & \mathbf{R}_{w2} & \cdots & \mathbf{R}_{ww} \end{bmatrix}, \tag{19}$$

where the (p,q)-th block \mathbf{R}_{pq} corresponds to the pair of candidates $(u_p,u_q)\in\mathcal{I}$. Substituting the explicit expressions of the AFDM time-domain samples into (19), and noting that $\mathbb{E}[\mathbf{s}_{(k)}] = \mathbb{E}[(\mathbf{A}\mathbf{x})_{(k)}] = 0$, the (m,m')-entry of \mathbf{R}_{pq} can be expressed as

$$\mathbf{R}_{pq(m,m')} = \frac{1}{N} e^{j2\pi c_1(m^2 - m'^2)} \times \sum_{n=0}^{N-1} \sum_{n'=0}^{N-1} \mathbb{E}[\mathbf{x}_{(n)}\mathbf{x}_{(n')}^*] e^{j2\pi \left(\alpha_{u_p}n^2 + \frac{m}{N}n - \alpha_{u_q}n'^2 - \frac{m'}{N}n'\right)}.$$
(20)

Considering that $\mathbb{E}\big[\mathbf{x}_{(n)}\mathbf{x}_{(n')}^*\big] = \delta_{n,n'}$, (20) can be simplified as

$$\mathbf{R}_{pq\,(m,m')} = \frac{1}{N} e^{j2\pi c_1(m^2 - m'^2)} \sum_{n=0}^{N-1} e^{j2\pi \left[(\alpha_{u_p} - \alpha_{u_q})n^2 + \frac{m - m'}{N}n \right]}.$$
(21)

From (21), the block correlation matrix \mathbf{R}_{pq} has the following properties.

Case w=1 (single candidate): When w=1, the stacked vector reduces to $\mathbf{s}_{\mathcal{I}}=\mathbf{s}_u\in\mathbb{C}^N$ and $\mathbf{R}_{\mathcal{I}}=\mathbf{I}_N$, i.e., no intra-candidate correlation.

Case w>1 (multiple candidates): Arrange $\mathbf{R}_{\mathcal{I}}$ as a $w\times w$ block matrix with $N\times N$ submatrices $\{\mathbf{R}_{pq}\}$.

- Diagonal blocks: For p = q, one obtains $\mathbf{R}_{pp} = \mathbf{I}_N$, indicating unit variance and no intra-candidate correlation.
- Off-diagonal blocks: For $p \neq q$, the magnitude of each entry depends only on the lag $\tau = m m'$.

Assuming further that the time-domain signals s_1, \ldots, s_U are mutually independent (no cross-candidate correlation), one has

$$\mathbf{R}_{\mathcal{I}} = \mathbf{I}_{wN}, \quad \text{for any } \mathcal{I} \subseteq \mathcal{U}.$$
 (22)

In this case, the CSM CCDF coincides with the independence expression (which is also the *theoretical lower bound*):

$$\bar{F}_{\mathcal{P}}^{\text{CSM}}(\gamma) = 1 - \Pr\left(\bigcup_{u=1}^{U} B_{u}(\gamma)\right)$$

$$= 1 - \sum_{w=1}^{U} (-1)^{w+1} \binom{U}{w} (1 - e^{-\gamma})^{wN}$$

$$= \left[1 - (1 - e^{-\gamma})^{N}\right]^{U}. \tag{23}$$

Motivated by diversity-order analyses for outage probability [36], [37], we define the *selection order* as the asymptotic decay rate of the PAPR CCDF

$$\mathcal{G}_{\text{sel}} \triangleq \lim_{\gamma \to \infty} \frac{-\ln \bar{F}_{\mathcal{P}}^{\text{CSM}}(\gamma)}{\gamma},$$
 (24)

For any $0 \le e^{-\gamma} \le 1$, Bernoulli's inequality and the binomial expansion yield

$$1 - Ne^{-\gamma} \le (1 - e^{-\gamma})^N \le 1 - Ne^{-\gamma} + {N \choose 2}e^{-2\gamma},$$
 (25)

which implies

$$Ne^{-\gamma} - \binom{N}{2}e^{-2\gamma} \le 1 - (1 - e^{-\gamma})^N \le Ne^{-\gamma}.$$
 (26)

Raising both sides to the power U,

$$(Ne^{-\gamma} - {N \choose 2}e^{-2\gamma})^U \le [1 - (1 - e^{-\gamma})^N]^U \le (Ne^{-\gamma})^U.$$
(27)

Taking logarithms and dividing by $\gamma > 0$ gives

$$U - \frac{U \ln N}{\gamma} - \frac{U}{\gamma} \ln \left(1 - \frac{N-1}{2} e^{-\gamma} \right) \ge \frac{-\ln \bar{F}_{\mathcal{P}}^{\text{CSM}}(\gamma)}{\gamma} \ge U - \frac{U \ln N}{\gamma}. \tag{28}$$

As $\gamma \to \infty$, both bounds in the inequality converge to U. Therefore, by the squeeze theorem,

$$\lim_{\gamma \to \infty} \frac{-\ln \bar{F}_{\mathcal{P}}^{\text{CSM}}(\gamma)}{\gamma} = U.$$
 (29)

Therefore, under the independence lower bound, the CCDF shows an exponential decay in the high-threshold regime. Equivalently, each independent candidate contributes one unit to the asymptotic decay rate.

IV. CHIRP PARAMETER CANDIDATE DESIGN

A. Chirp Parameter Candidate Design Criteria

To approach the theoretical lower bound in (23), the candidate set \mathcal{A} must be carefully designed. As shown in (22), this requires that for any pair of distinct candidates $p \neq q$, the corresponding block \mathbf{R}_{pq} should ideally equal the zero matrix. More specifically, the (m,m')-entry of \mathbf{R}_{pq} depends only on the lag $\tau=m-m'$ and can be written in terms of

$$C(\tau) \triangleq \frac{1}{N} \sum_{n=0}^{N-1} e^{j2\pi(\Delta \alpha n^2 + \frac{\tau}{N}n)}, \quad \Delta \alpha = \alpha_{u_p} - \alpha_{u_q}, \quad (30)$$

where the ideal condition $\mathbf{R}_{pq} = \mathbf{0}_N$ would correspond to $C(\tau) = 0$ for all τ . Note that the criterion in (30) differs from the parameter design rule in [32]: while [32] only accounts for the correlation across different candidates at the same time index, (30) additionally captures the cross-candidate correlations across different time lags.

However, as will be shown next, such a strict condition cannot hold in general. This observation is formalized in the following proposition and can be readily extended to other phase-selection-based AFDM designs.

Proposition 1: For any deterministic chirp difference $\Delta \alpha$, there exists at least one $\tau \in \{0, 1, \dots, N-1\}$ such that

$$C(\tau) \neq 0. \tag{31}$$

Equivalently,

$$\exists \Delta \alpha \in \mathbb{R}, \quad \text{s.t. } C(\tau) = 0, \ \forall \tau.$$
(32)

Proof: By rewriting $C(\tau)$ as the scaled DFT of the sequence

$$a_n = e^{j2\pi\Delta\alpha n^2}, \quad n = 0, 1, \dots, N - 1,$$

we obtain

$$C(\tau) = \frac{1}{N} \sum_{n=0}^{N-1} a_n e^{j\omega_{\tau} n}, \quad \omega_{\tau} = 2\pi \frac{\tau}{N}.$$
 (33)

If $C(\tau) = 0$ for all τ , then by the inverse DFT,

$$a_n = \sum_{\tau=0}^{N-1} C(\tau) e^{-j\omega_{\tau} n} = 0,$$
 (34)

which contradicts $|a_n|=1$ for all n. Hence the claim follows.

Therefore, rather than enforcing the strict criterion in (30), we relax it to an asymptotic one given by:

$$\lim_{N \to \infty} C(\tau) = 0, \forall \tau \in \{0, 1, \dots, N - 1\}.$$
 (35)

B. Practical Guidelines for Designing A

Under the design criteria specified in (35), the design of \mathcal{A} can be approached in various ways, such as optimization-based methods, heuristic searches, or exhaustive enumeration. From a practical standpoint and to reduce computational complexity, we exploit the properties of generalized quadratic Gaussian sums to simplify the design of \mathcal{A} .

Proposition 2: (Bound on GQGS): Let

$$G(f,g,h) = \sum_{n=0}^{h-1} e^{\frac{2\pi j}{h} \left(fn^2 + gn\right)}.$$

where $f, g, h \in \mathbb{Z}$ and h > 0. If $h \equiv 0 \pmod{4}$, then

$$|G(f,g,h)| \le \sqrt{2h}, \quad \forall f \text{ with } \gcd(f,h) = 1.$$
 (36)

Proof: Please refer to Appendix A.

The structure of $C(\tau)$ in (21) closely resembles a GQGS. To make this connection precise, we first rewrite it in the following form:

$$C(\tau) = \frac{1}{N} \sum_{n=0}^{N-1} e^{\frac{2\pi j}{2N} \left[(2N\Delta\alpha)n^2 + 2\tau n \right]}.$$
 (37)

Assuming that $2N\Delta\alpha \in \mathbb{Z}$, this summation, up to the prefactor 1/N, has the same quadratic form as the generalized Gauss sum G(f, g, h) introduced in Proposition 2, with parameters¹

$$f = 2N\Delta\alpha$$
, $q = 2\tau$, $h = 2N$

except that in $C(\tau)$ the summation is truncated to the first N terms $(0 \le n \le N-1)$ instead of covering the full range $(0 \le n \le 2N-1)$.

Partitioning the full sum into two segments and changing variables n' = n - N gives

$$G(f,g,2N) = \sum_{n=0}^{N-1} e^{\frac{2\pi j}{2N}(fn^2+gn)} + \sum_{n=N}^{2N-1} e^{\frac{2\pi j}{2N}(fn^2+gn)}$$

$$= \sum_{n=0}^{N-1} e^{\frac{2\pi j}{2N}(fn^2+gn)} + \sum_{n'=0}^{N-1} e^{\frac{2\pi j}{2N}\left(f(n'+N)^2+g(n'+N)\right)}$$

$$= \left(1 + e^{j\pi(fN+g)}\right) \sum_{n=0}^{N-1} e^{\frac{2\pi j}{2N}(fn^2+gn)}.$$
(38)

Noting that $fN + g = 2(N^2\Delta\alpha + \tau)$ is even, we obtain

$$|C(\tau)| = \frac{1}{2N} |G(2N\Delta\alpha, 2\tau, 2N)|. \tag{39}$$

To further characterize this Gaussian sum, let $d=\gcd(2N\Delta\alpha,2N)$. If $d\nmid 2\tau$, then $G(2N\Delta\alpha,2\tau,2N)=0$. If instead $d\mid 2\tau$, we can write

$$2N\Delta\alpha = df_1$$
, $2\tau = dg_1$, $2N = dh_1$,

with $gcd(f_1, h_1) = 1$. By the Gauss sum reduction formula (see [38]),

$$G(2N\Delta\alpha, 2\tau, 2N) = d \cdot G(f_1, g_1, h_1). \tag{40}$$

Using Propostion 2, the magnitude satisfies

$$|G(f_1, g_1, h_1)| \le \sqrt{2h_1} = 2\sqrt{N/d},$$
 (41)

and hence

$$|C(\tau)| = \frac{d}{2N} |G(f_1, g_1, h_1)| \le \sqrt{d/N}.$$
 (42)

Therefore, as $\sqrt{d/N} \to 0$, (35) becomes asymptotically valid. This observation provides practical insight for the design of candidate sets \mathcal{A} under the constraint $2N\Delta_q \in \mathbb{Z}$: to achieve low cross-covariance, the chirp parameters should be chosen to keep the pairwise values of

$$d_{p,q} = \gcd(2N(\alpha_{u_p} - \alpha_{u_q}), 2N), \quad \forall \alpha_{u_p} \neq \alpha_{u_q} \in \mathcal{A}$$

as small as possible across all sequence pairs.

In practical scenarios, a significant reduction in PAPR can often be achieved without a large candidate set size U [30]. Ideally, one would prefer $\max_{p\neq q} d_{p,q} = 1$, i.e., all pairwise differences being odd. However, as U increases, it becomes impossible to guarantee that every pairwise difference is odd; even differences inevitably appear. Moreover, the magnitude of these even differences grows with U, which in turn increases the worst-case value of $d_{p,q}$. Therefore, the proposed CSM scheme is particularly effective when $U \ll N$. As an illustrative design example in the regime $U \ll N$, we consider

$$\alpha_u = \frac{u-1}{2N}, \quad u = 1, \dots, U, \tag{43}$$

for which the worst-case pairwise gcd can be expressed as

$$d_{\max} \triangleq \max_{p \neq q} d_{p,q} = 2^{\lfloor \log_2(U-1) \rfloor}. \tag{44}$$

This construction provides a simple yet effective candidate set with predictable cross-covariance behavior.

 $^{^1}$ In practical communication systems N is typically a power of two; hence for large subcarrier numbers we assume $h=2N\equiv 0\pmod 4$.

TABLE I: Complexity comparison

Assumes radix-2 IFFT implementation; CSM and GPS consider U candidates.

Scheme	Complex multiplications	Complex additions
CSM	$\frac{UN}{2}\log_2 N + (U+1)N$	$UN \log_2 N$
GPS	$\frac{UN}{2}\log_2 N + (U+1)N$ $\frac{UN}{2}\log_2 N + 2UN$	$UN\log_2 N$
HC-WAFT	$\frac{N}{2}\log_2 N + 6N$	$N\log_2 N + 3N$

V. SIMULATION RESULTS

In this section, we present numerical results to validate the proposed CSM scheme for PAPR reduction in AFDM systems.

A. Simulation Setup

Unless otherwise specified, the number of subcarriers is set to N=512, and QPSK constellation is employed. The default candidate set for the chirp parameters follows the design in (43) with U=4 candidates. Each CCDF curve is obtained by averaging over 10^7 independent Monte Carlo trials to ensure statistical reliability.

We consider two baseline algorithms to benchmark the proposed CSM scheme for PAPR reduction in AFDM systems. The first baseline is GPS [32], where the candidate set is generated by dividing the pre-chirp parameters into W groups, each providing V candidates. To ensure fairness, the GPS parameters are designed such that $W^V=U$, i.e., the total number of candidates is matched to CSM, and thus all schemes require $\log_2 U$ bits of side information. The second baseline is HC-WAFT [33], in which the system is configured by a pair of parameters $(\alpha_{\rm HC}, \beta_{\rm HC})$. By decreasing $\alpha_{\rm HC}$ towards zero, the relative weight of the embedded single-carrier component is increased, which effectively suppresses signal peaks and reduces the PAPR.

To further assess the practicality of CSM relative to these baselines, we compare their computational complexities. Since all three schemes rely on IFFT operations, their dominant complexity scales on the order of $N\log N$. Nevertheless, the additional operations differ across algorithms, which leads to non-negligible differences in the actual number of complex multiplications and additions. For a more precise comparison, Table I summarizes the operation counts under radix-2 IFFT implementation, assuming U candidate sequences.

B. Results and Discussion

We first examine the impact of candidate set design on the PAPR performance of AFDM-CSM, as illustrated in Fig. 3. The achievable PAPR reduction largely depends on the design of the candidate set, highlighting the importance of careful set design. With the design in (43), the simulated CCDF closely approaches the theoretical lower bound. At CCDF = 10^{-4} , AFDM-CSM with the design in (43) achieves about 2.6 dB improvement over conventional AFDM. For this set, $d_{\rm max}=3$. For comparison, we also consider uniformly spaced candidates of the form $\alpha_u=\frac{s(u-1)}{2N},\ u=1,\ldots,U,$ where $s\in\{16,64,256\}$. In these cases, $d_{\rm max}=s-1$, i.e., 15, 63, and 255, respectively. As shown in Fig. 3, the PAPR reduction gradually deteriorates as $d_{\rm max}$ increases, reflecting

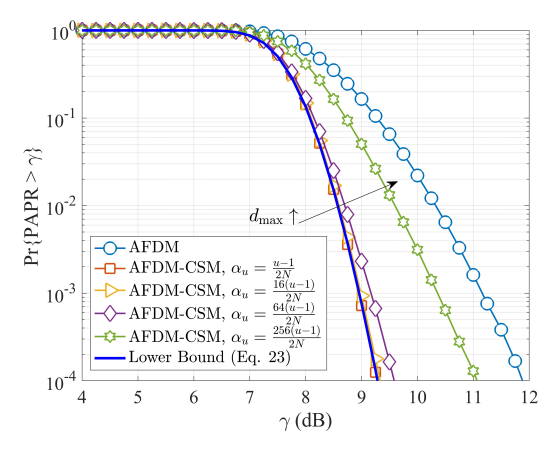


Fig. 3: CCDF of PAPR for AFDM-CSM under different candidate set designs.

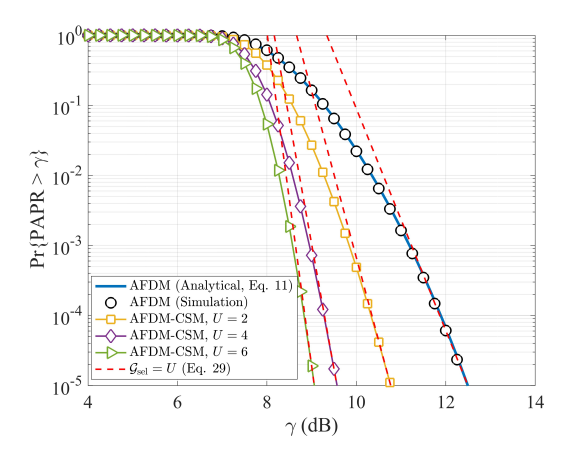


Fig. 4: CCDF comparison of PAPR for AFDM and AFDM-CSM with different candidate set sizes.

stronger cross-candidate correlation (cf. the covariance indicator $C(\tau)$) and thus a larger deviation from the independence lower bound. Notably, when $\alpha_u = \frac{256(u-1)}{2N}$, the performance improvement is less than 1 dB at 10^{-4} CCDF, indicating that excessive candidate correlation severely limits the achievable PAPR reduction.

We then evaluate the CCDF of the PAPR for conventional AFDM and AFDM-CSM with different candidate set sizes, as shown in Fig. 4. Under the large-N assumption, the CCDF of conventional AFDM closely matches the theoretical curve derived from the CLT approximation, confirming that AFDM, similar to OFDM, inherits the high-PAPR drawback of multicarrier systems. By introducing multiple c_2 candidates in CSM, the PAPR performance can be significantly improved. Furthermore, conventional AFDM can be regarded as the special case of CSM with U=1, and increasing U consistently leads to further PAPR reduction. The analytical expression in (29) shows a close match with the simulation results in the high threshold regime. This confirms that the proposed design effectively approaches the full selection-order behavior of the transmitted signal, thereby validating its effectiveness across different candidate set sizes.

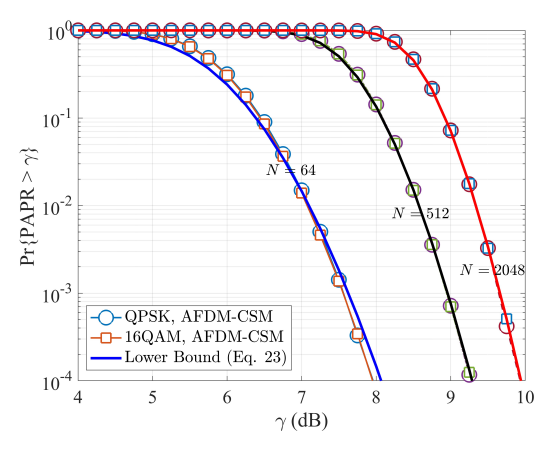


Fig. 5: CCDF of PAPR for AFDM-CSM with different subcarrier settings.

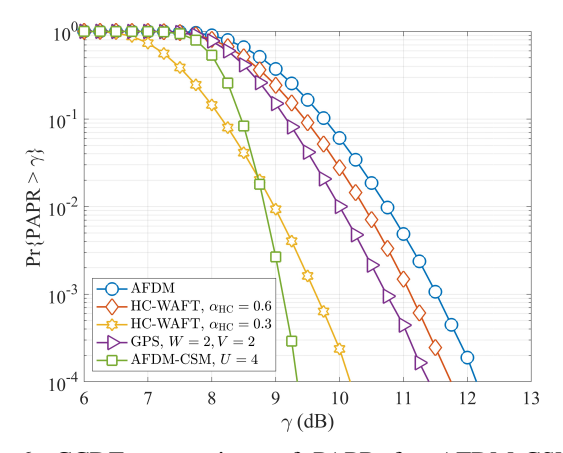


Fig. 6: CCDF comparison of PAPR for AFDM-CSM and baseline schemes.

Fig. 5 presents the CCDF performance of CSM under different subcarrier settings. The results for QPSK and 16QAM are almost identical. This phenomenon can be explained by CLT: when the number of subcarriers N is large, the superposition of many independently subcarriers makes the time-domain AFDM samples approximately Gaussian, and hence the modulation format has little impact on the PAPR statistics. As N increases, the PAPR of CSM also grows, but the CCDF curve progressively approaches the theoretical lower bound. For smaller subcarrier sizes, however, a noticeable deviation from the bound can be observed. This deviation mainly arises from two factors: (i) the Gaussian approximation in the time domain becomes less accurate for small N, and (ii) the crosscandidate correlation term $C(\tau)$ in (36) remains significant, limiting the validity of the independence assumption.

The preceding simulations are conducted at the Nyquist sampling rate, which offers low computational complexity and still reflects the relative performance differences among the schemes. These results can therefore serve as a useful reference. Nevertheless, Nyquist-rate signals may not fully capture the true peaks of the continuous-time waveform. To obtain a more accurate approximation of the continuous-time

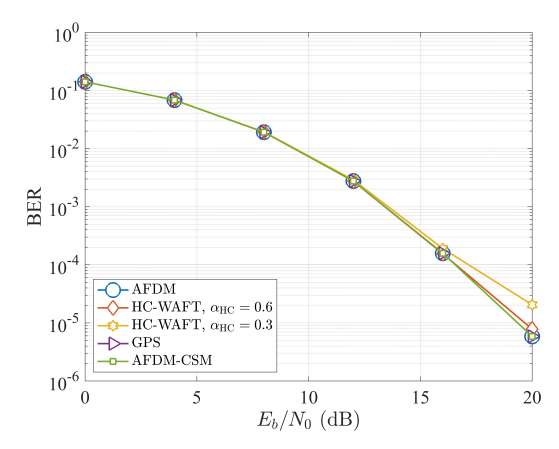


Fig. 7: BER performance comparison of AFDM-CSM and baseline schemes under the EVA channel.

behavior, the signal is typically oversampled by inserting zeros in the frequency domain and applying a higher-point inverse DFT. In practice, an oversampling factor of $L \geq 4$ is widely adopted as sufficient [39], [40]. Accordingly, we also provide oversampled simulation results to complement the Nyquistrate analysis and to more faithfully characterize the actual PAPR performance.

Fig. 6 shows the CCDF performance of PAPR for CSM and the baseline schemes under four-times oversampling with U=4, corresponding to 2 bits of side information. It can be clearly observed that the proposed CSM outperforms GPS. This is because the GPS design does not explicitly account for the cross-lag correlation between different sequences; as a result, some candidate sequences may exhibit strong temporal correlation, preventing GPS from fully realizing its potential PAPR reduction. For HC-WAFT, we consider weighting parameters $\alpha_{\rm HC}=0.3$ and 0.6. As $\alpha_{\rm HC}$ decreases towards zero, the relative proportion of single-carrier components increases while the multicarrier contribution diminishes, which explains why $\alpha_{\rm HC} = 0.3$ achieves better PAPR performance than $\alpha_{\rm HC}=0.6$. Nevertheless, since HC-WAFT is not based on a selective mapping mechanism, its CCDF curve exhibits a different decay behavior. Specifically, when $\gamma < 8.7$ dB, HC-WAFT with $\alpha_{\rm HC}=0.3$ achieves lower PAPR than CSM, but for $\gamma > 8.7$ dB the proposed CSM yields superior performance. In the high-PAPR regime, it shows a diversitylike slope due to the multi-candidate selection gain. Overall, these results highlight that GPS is fundamentally limited by candidate correlation, HC-WAFT and CSM show complementary strengths in different operating regions.

As a complement to Fig. 6, Fig. 7 illustrates the BER performance of AFDM-CSM and the baseline schemes. The simulation assumes a carrier frequency of 9 GHz, a subcarrier spacing of 30 kHz, and a maximum normalized Doppler of 0.15 under the EVA channel model, which represents a typical doubly selective fading environment. The results show that both GPS and CSM preserve the BER performance of AFDM without introducing noticeable degradation. In contrast, HC-WAFT exhibits a slight performance loss when the proportion of single-carrier components is increased: for $E_b/N_0 > 16 \, \mathrm{dB}$,

the BER curve deviates downward, reflecting reduced robustness against doubly selective fading. This indicates that while HC-WAFT can suppress peaks, it inevitably introduces a new trade-off in terms of reliability. Taken together, Fig. 6 and Fig. 7 demonstrate that AFDM-CSM achieves significant PAPR reduction with only a small amount of side information, while fully preserving the BER performance of the underlying AFDM system.

VI. CONCLUSION

This work introduced CSM as an effective approach for reducing the PAPR of AFDM systems. We showed that, by properly designing the c_2 candidate set, CSM can closely approach the theoretical lower bound derived from the independence assumption. Asymptotic analysis and simulation results consistently indicate that CSM approximately achieves a selection-order gain. Compared with GPS and HC-WAFT baselines, CSM achieves superior PAPR reduction while maintaining the same BER performance. Since CSM operates solely via selected mapping of the signal-side parameter c_2 without altering the channel-side parameter c_1 , it effectively decouples PAPR control from channel-related BER optimization, enabling a practical and robust waveform design for AFDM systems. Overall, CSM contributes to more efficient utilization of the RF hardware resources in AFDM implementations, and future work may extend the framework to joint design with coding or multiple-antenna systems.

APPENDIX A PROOF OF PROPOSITION 2

Consider the quadratic exponential sum

$$G(f,g,h) = \sum_{n=0}^{h-1} \exp\left(\frac{2\pi i}{h}(fn^2 + gn)\right),$$
 (45)

with $f, g, h \in \mathbb{Z}$, h > 0, and gcd(f, h) = 1. We show that for $h \equiv 0 \pmod{4}$ it holds that

$$|G(f,g,h)| \le \sqrt{2h}. (46)$$

If g is odd, pairing n with n + h/2 yields

$$G(f,g,h) = \sum_{n=0}^{h/2-1} e^{2\pi i (fn^2 + gn)/h} (1 + e^{\pi i g}) = 0.$$
 (47)

If g = 2m is even, completing the square gives

$$G(f, 2m, h) = g_1(f, h) e_h(-fm^2),$$
 (48)

where

$$g_1(f,h) = \sum_{n=0}^{h-1} e^{2\pi i f n^2/h}$$
 (49)

is the classical quadratic Gauss sum. Its absolute value is given by the following standard result (see, e.g., [41], [42]):

$$|g_1(f,h)| = \begin{cases} \sqrt{h}, & h \text{ odd,} \\ 2^{(t+1)/2}, & h = 2^t, \ t \ge 2, \\ 0, & h \equiv 2 \pmod{4}. \end{cases}$$
 (50)

Since in practical systems the number of subcarriers is typically a power of two, we focus on the case $h=2^t$ with t > 2, so that

$$|G(f,g,h)| = |g_1(f,h)| = 2^{(t+1)/2} = \sqrt{2h}.$$
 (51)

Combining the two cases of g being odd and even, we obtain

$$|G(f,g,h)| \le \sqrt{2h},$$

which completes the proof of Proposition 2.

REFERENCES

- [1] C.-X. Wang, X. You, X. Gao, X. Zhu, Z. Li, C. Zhang, H. Wang, Y. Huang, Y. Chen, H. Haas, J. S. Thompson, E. G. Larsson, M. D. Renzo, W. Tong, P. Zhu, X. Shen, H. V. Poor, and L. Hanzo, "On the road to 6G: Visions, requirements, key technologies, and testbeds," *IEEE Commun. Surv. Tutorials*, vol. 25, no. 2, pp. 905–974, 2023.
- [2] A. Bemani, N. Ksairi, and M. Kountouris, "Affine frequency division multiplexing for next generation wireless communications," *IEEE Trans. Wireless Commun.*, vol. 22, no. 11, pp. 8214–8229, Mar. 2023.
- [3] Z. Li, C. Zhang, G. Song, X. Fang, X. Sha, and D. T. M. Slock, "Chirp parameter selection for affine frequency division multiplexing with mmse equalization," *IEEE Trans. Commun.*, vol. 73, no. 7, pp. 5079–5093, 2025.
- [4] W. Benzine, A. Bemani, N. Ksairi, and D. Slock, "Affine frequency division multiplexing for communications on sparse time-varying channels," in *Proc. IEEE Global Commun. Conf. (GLOBECOM)*, 2023, pp. 4921–4926.
- [5] P. Raviteja, Y. Hong, E. Viterbo, and E. Biglieri, "Practical pulse-shaping waveforms for reduced-cyclic-prefix OTFS," *IEEE Transactions on Vehicular Technology*, vol. 68, no. 1, pp. 957–961, Oct. 2019.
- [6] Q. Luo, P. Xiao, Z. Liu, Z. Wan, N. Thomos, Z. Gao, and Z. He, "AFDM-SCMA: A promising waveform for massive connectivity over high mobility channels," *IEEE Trans. Wireless Commun.*, vol. 23, no. 10, pp. 14421–14436, Jun. 2024.
- [7] Z. Sui, Z. Liu, L. Musavian, L.-L. Yang, and L. Hanzo, "Generalized spatial modulation aided affine frequency division multiplexing," *IEEE Trans. Wireless Commun.*, early access, 2025, doi: 10.1109/TWC.2025.3613062.
- [8] J. Zhu, Y. Tang, F. Liu, X. Zhang, H. Yin, and Y. Zhou, "AFDM-based bistatic integrated sensing and communication in static scatterer environments," *IEEE Wireless Communications Letters*, vol. 13, no. 8, pp. 2245–2249, Aug. 2024.
- [9] H. Yin, Y. Tang, Y. Ni, Z. Wang, G. Chen, J. Xiong, K. Yang, M. Kountouris, Y. L. Guan, and Y. Zeng, "Ambiguity function analysis of AFDM signals for integrated sensing and communications," *IEEE J. Sel. Areas Commun.*, early access, 2025, doi: 10.1109/JSAC.2025.3611936.
- [10] F. Zhang, Z. Wang, T. Mao, T. Jiao, Y. Zhuo, M. Wen, W. Xiang, S. Chen, and G. K. Karagiannidis, "AFDM-enabled integrated sensing and communication: Theoretical framework and pilot design," *IEEE J. Sel. Areas Commun.*, early access, 2025, doi: 10.1109/JSAC.2025.3609766.
- [11] D. Stojanović, I. Djurović, and B. R. Vojcic, "Multicarrier communications based on the affine Fourier transform in doubly dispersive channels," *EURASIP J. Wireless Commun. Networking*, vol. 2010, no. 1, Art. no. 868314, Dec. 2010.
- [12] S. H. Han and J. H. Lee, "An overview of peak-to-average power ratio reduction techniques for multicarrier transmission," *IEEE Wireless Commun.*, vol. 12, no. 2, pp. 56–65, Apr. 2005.
- [13] T. Jiang and Y. Wu, "An overview: Peak-to-average power ratio reduction techniques for OFDM signals," *IEEE Trans. Broadcast.*, vol. 54, no. 2, pp. 257–268, Jun. 2008.
- [14] J. Joung, C. K. Ho, and S. Sun, "Spectral efficiency and energy efficiency of OFDM systems: Impact of power amplifiers and countermeasures," *IEEE J. Sel. Areas Commun.*, vol. 32, no. 2, pp. 208–220, Feb. 2014.
- [15] D. Kim and S. An, "Experimental analysis of PAPR reduction technique using hybrid peak windowing in LTE system," EURASIP J. Wireless Commun. Networking, vol. 2015, no. 1, Art. no. 75, Mar. 2015.
- [16] Y. Rahmatallah and S. Mohan, "Peak-to-average power ratio reduction in OFDM systems: A survey and taxonomy," *IEEE Commun. Surveys Tuts.*, vol. 15, no. 4, pp. 1567–1592, Fourth Quart. 2013.
- [17] A. Cheaito, J.-F. Hélard, M. Crussière, and Y. Louët, "EVM derivation of multicarrier signals to determine the operating point of the power amplifier considering clipping and predistortion," EURASIP J. Wireless Commun. Networking, vol. 2016, no. 1, Art. no. 281, Dec. 2016.

- [18] A. Tom, A. Şahin, and H. Arslan, "Suppressing alignment: Joint PAPR and out-of-band power leakage reduction for OFDM-based systems," *IEEE Trans. Commun.*, vol. 64, no. 3, pp. 1100–1109, Mar. 2016.
- [19] T. Kageyama, O. Muta, and H. Gacanin, "Performance analysis of OFDM with peak cancellation under EVM and ACLR restrictions," *IEEE Trans. Veh. Technol.*, vol. 69, no. 6, pp. 6230–6241, Jun. 2020.
- [20] Y. Wang and A. N. Akansu, "Low-complexity peak-to-average power ratio reduction method for orthogonal frequency-division multiplexing communications," *IET Commun.*, vol. 9, no. 17, pp. 2153–2159, Nov. 2015.
- [21] S. H. Leung, S. M. Ju, and G. G. Bi, "Algorithm for repeated clipping and filtering in peak-to-average power reduction for OFDM," *Electron. Lett.*, vol. 38, no. 25, pp. 1726–1727, Dec. 2002.
- [22] T. Jiang, Y. Yang, and Y.-H. Song, "Exponential companding technique for PAPR reduction in OFDM systems," *IEEE Trans. Broadcast.*, vol. 51, no. 2, pp. 244–248, Jun. 2005.
- [23] S. H. Muller and J. B. Huber, "OFDM with reduced peak-to-average power ratio by optimum combination of partial transmit sequences," *Electron. Lett.*, vol. 33, no. 5, pp. 368–369, Feb. 1997.
- [24] J. Hou, J. Ge, and J. Li, "Peak-to-average power ratio reduction of OFDM signals using PTS scheme with low computational complexity," *IEEE Trans. Broadcast.*, vol. 57, no. 1, pp. 143–148, Mar. 2011.
- [25] R. Sayyari, J. Pourrostam, and H. Ahmadi, "A low-complexity PTS-based PAPR reduction method for the downlink of OFDM-NOMA systems," in *Proc. IEEE Wireless Commun. Netw. Conf. (WCNC)*, Apr. 2022, pp. 1719–1724.
- [26] L. Mei, X. Sha, and N. Zhang, "PAPR of hybrid carrier scheme based on weighted-type fractional Fourier transform," in *Proc. 6th Int. ICST Conf. Commun. Netw. China (CHINACOM)*, Aug. 2011, pp. 237–240.
- [27] I. Cinemre, V. Aydin, and G. Hacioglu, "PAPR reduction through Gaussian pre-coding in DCO-OFDM systems," Opt. Quantum Electron., vol. 56, no. 6, Art. no. 958, Apr. 2024.
- [28] Z. P. Wang, J. N. Xiao, F. Li, and L. Chen, "Hadamard precoding for PAPR reduction in optical direct detection OFDM systems," *Optoelectron. Lett.*, vol. 7, no. 5, pp. 363–366, Sept. 2011.
- [29] R. W. Bauml, R. F. H. Fischer, and J. B. Huber, "Reducing the peak-to-average power ratio of multicarrier modulation by selected mapping," *Electron. Lett.*, vol. 32, no. 22, pp. 2056–2057, Oct. 1996.
- [30] S. H. Han and J. H. Lee, "Modified selected mapping technique for PAPR reduction of coded OFDM signal," *IEEE Trans. Broadcast.*, vol. 50, no. 3, pp. 335–341, Sept. 2004.
- [31] V. Savaux, "Peak to average power ratio reduction techniques based on chirp selection for single and multi-user orthogonal chirp division multiplexing system," *IET Signal Process.*, vol. 17, no. 5, Art. no. e12215, May 2023.
- [32] H. Yuan, Y. Xu, X. Guo, Y. Ge, T. Ma, H. Li, D. He, and W. Zhang, "PAPR reduction with pre-chirp selection for affine frequency division multiplexing," *IEEE Wireless Commun. Lett.*, vol. 14, no. 3, pp. 736–740, Mar. 2025.
- [33] Z. Li, L. Ou, C. Zhang, X. Fang, and X. Sha, "A hybrid carrier communication system based on weighted affine Fourier transform," *IEEE Commun. Lett.*, vol. 28, no. 7, pp. 1629–1633, Jul. 2024.
- [34] V. M. Reddy and H. Bitra, "PAPR in AFDM: Upper bound and reduction with normalized μ -law companding," *IEEE Access*, vol. 13, pp. 86553–86561, May 2025.
- [35] T. Erseghe, N. Laurenti, and V. Cellini, "A multicarrier architecture based upon the affine Fourier transform," *IEEE Trans. Commun.*, vol. 53, no. 5, pp. 853–862, May 2005.
- [36] H. Zhao and D. Slock, "Analytical insights into outage probability and ergodic capacity of fluid antenna systems," *IEEE Wireless Commun. Lett.*, vol. 14, no. 5, pp. 1581–1585, May 2025.
- [37] W. K. New, K.-K. Wong, H. Xu, K.-F. Tong, and C.-B. Chae, "Fluid antenna system: New insights on outage probability and diversity gain," *IEEE Trans. Wireless Commun.*, vol. 23, no. 1, pp. 128–140, Jan. 2024.
- [38] B. C. Berndt, R. J. Evans, and K. S. Williams, Gauss and Jacobi Sums. New York, NY, USA: Wiley, Jun. 1998.
- [39] C. Tellambura, "Computation of the continuous-time PAR of an OFDM signal with BPSK subcarriers," *IEEE Commun. Lett.*, vol. 5, no. 5, pp. 185–187, May 2002.
- [40] K. D. Wong, M.-O. Pun, and H. V. Poor, "The continuous-time peak-to-average power ratio of OFDM signals using complex modulation schemes," *IEEE Trans. Commun.*, vol. 56, no. 9, pp. 1390–1393, Sept. 2008
- [41] E. D. Akarsu and J. Marklof, "The value distribution of incomplete Gauss sums," *Mathematika*, vol. 59, no. 2, pp. 381–398, Jul. 2013.
- [42] K. I. Oskolkov, "On functional properties of incomplete Gaussian sums," Can. J. Math., vol. 43, no. 1, pp. 182–212, Feb. 1991.